

Modeling individual-specific human optic nerve head biomechanics. Part I: IOP-induced deformations and influence of geometry

Ian A. Sigal · John G. Flanagan · Inka Tertinegg ·
C. Ross Ethier

Received: 12 April 2007 / Accepted: 29 January 2008 / Published online: 29 February 2008
© Springer-Verlag 2008

Abstract Glaucoma, the second most common cause of blindness worldwide, is an ocular disease characterized by progressive loss of retinal ganglion cell (RGC) axons. Biomechanical factors are thought to play a central role in RGC loss, but the specific mechanism underlying this disease remains unknown. Our goal was to characterize the biomechanical environment in the optic nerve head (ONH)—the region where RGC damage occurs—in human eyes. Post mortem human eyes were imaged, fixed at either 5 or 50 mmHg pressure and processed histologically to acquire serial sections through the ONH. Three-dimensional models of the ONH region were reconstructed from these sections and embedded in a generic scleral shell to create a model of an entire eye. We used finite element simulations to quantify the effects of

an acute change in intraocular pressure from 5 to 50 mmHg on the ONH biomechanical environment. Computed strains varied substantially within the ONH, with the pre-laminar neural tissue and the lamina cribrosa showing the greatest strains. The mode of strain having the largest magnitude was third principal strain (compression), reaching 12–15% in both the lamina cribrosa and the pre-laminar neural tissue. Shear strains were also substantial. The distribution of strains in all ONH tissues was remarkably similar between eyes. Inter-individual variations in ONH geometry (anatomy) have only modest effects on ONH biomechanics, and may not explain inter-individual susceptibility to elevated intraocular pressure. Consistent with previous results using generic ONH models, the displacements of the vitreo-retinal interface and the anterior surface of the lamina cribrosa can differ substantially, suggesting that currently available optical imaging methods do not provide information of the acute deformations within ONH tissues. Predicted strains within ONH tissues are potentially biologically significant and support the hypothesis that biomechanical factors contribute to the initial insult that leads to RGC loss in glaucoma.

Ian A. Sigal now a post-doctoral research fellow at Ocular Biomechanics Laboratory, Devers Eye Institute, Legacy Health Research. Portland, OR, USA. (isigal@deverseye.org).

I. A. Sigal · C. R. Ethier
Department of Mechanical & Industrial Engineering,
University of Toronto, Toronto, Canada

I. A. Sigal · C. R. Ethier
Institute for Biomaterials and Biomedical Engineering,
University of Toronto, Toronto, Canada

J. G. Flanagan · I. Tertinegg · C. R. Ethier
Department of Ophthalmology and Vision Sciences,
University of Toronto, Toronto, Canada

J. G. Flanagan
School of Optometry, University of Waterloo, Waterloo, Canada

C. R. Ethier (✉)
Department of Bioengineering, Imperial College London,
London SW7 2AZ, UK
e-mail: r.ethier@imperial.ac.uk

Keywords Biomechanics · Glaucoma · Optic nerve head · IOP · Finite elements · Strain · Sclera · Lamina cribrosa

1 Introduction

Glaucoma is an ocular disease that is the second most common cause of blindness worldwide. It is projected that glaucoma will affect approximately 50 million people worldwide in 2010, rising to 80 million in 2020 (Quigley and Broman 2006). Glaucoma is an optic neuropathy, in which retinal ganglion cells—responsible for transmission of information from the retina to the lateral geniculate nucleus, enroute

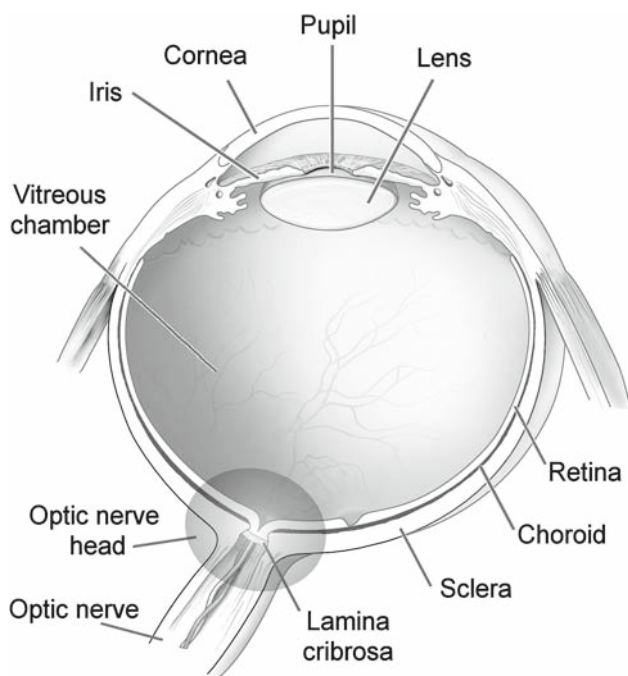


Fig. 1 Schematic cross-section through a human eye. Light enters the eye through the cornea, passes through the pupil, lens and vitreous humour and strikes the retina. Retinal nerve fibres transmit visual information to the brain. These fibres converge at the optic nerve head region, exit the eye through the scleral canal, and form the optic nerve. The lamina cribrosa is a porous structure that spans the scleral canal. The vitreous chamber is filled with the vitreous humor, which exerts a pressure on the surface of the retina (the pre-laminar neural tissue). Adapted from a diagram by the National Eye Institute

to the visual cortex—become dysfunctional and eventually undergo apoptosis or possibly other modes of programmed self-destruction (Whitmore et al. 2005). Clinically, this process results in a characteristic pattern of visual field loss and changes in the shape and appearance of the optic nerve head (ONH), the site in the eye where retinal ganglion cell axons converge before leaving the posterior eye through the scleral canal (see Fig. 1 for ocular anatomy).

The primary risk factor for the development of glaucomatous optic neuropathy is elevated intraocular pressure (IOP), and significant, sustained IOP reduction is known to preserve vision (Heijl et al. 2002). This clinical observation, in conjunction with many others (Burgoyne et al. 2005), strongly suggests that biomechanical factors acting within the ONH contribute to the pathogenesis of glaucomatous optic neuropathy (Ethier et al. 2004). In this regard, significant attention has been focussed on the biomechanics of the lamina cribrosa (LC), a porous connective tissue spanning the scleral canal through which retinal ganglion cell axons pass as they exit the eye (Bellezza 2002, Burgoyne et al. 2004, 2005, Downs 2002, Edwards et al. 2001, Ethier et al. 2004, Hernandez 2000, Levy et al. 1981, Levy and Crapps 1984,

Morgan et al. 1995, 2002). It is hypothesized that extension, compression or shearing of retinal ganglion cells axons, or of the astrocytes within the lamina cribrosa, contribute to the loss of neural function in glaucoma (Sigal et al. 2007, 2008).

Unfortunately, the relationship between IOP and the risk of developing glaucoma is not straightforward, since the level of IOP that leads to glaucomatous optic neuropathy varies between individuals. The reason for this range of sensitivity to IOP is unclear, but may stem from inter-individual differences in optic nerve head biomechanics, possibly due to variations in geometry (anatomy) and material properties between ONHs. Unfortunately, since the ONH is difficult to access directly, a full characterization of the influence of geometry and material properties on the biomechanical response of the ONH to changes in IOP has remained elusive.

We previously studied the influence of various factors, including geometric factors such as scleral thickness and ONH size, on the biomechanics of the ONH (Sigal et al. 2005a). However, that study had several limitations. First, the models were generic and axisymmetric, and therefore did not represent the complex 3D architecture of a real ONH. Second, the geometric factors studied were varied independently over ranges determined from the literature. It is possible that there are interactions between the geometric factors, and although a meta-study (Sigal et al. 2005a) on the influence of factor range suggested a modest effect, it is still possible that the choice of factor ranges biased the results. Third, only the maximum tissue extension (the first principal strain) was considered during the analysis of the mechanical response. However, in (Sigal et al. 2007, 2008) it was shown that other modes of strain in the ONH frequently have larger magnitude than the first principal strain, and therefore maximum tissue compression (third principal strain), and maximum shearing strain should also be examined.

This study addresses these limitations using finite element modeling (FEM) to study the biomechanics of individual-specific human optic nerve heads and by considering more complete characterizations of strain distributions than have been previously presented.

2 Methods

2.1 Model construction and simulations

2.1.1 Geometry

Ten eyes from six donors were used (Table 1) to construct ONH models, including three models that were previously used (Sigal et al. 2007, 2008). Eyes were obtained from the Eye Bank of Canada (Ontario division, Toronto) and

Table 1 Summary of donor information and model properties

Donor/model	1	1	2	3	4	4	5	5	6	6	Generic
Age (years)		83	79	91		76		84		70	–
Gender		M	M	M		M		M		M	–
Time to enucleation (Hrs)		2	2	10		3		7		7	–
Time to imaging (Hrs)		17	23.5	29		19		24		16	–
Eye	OD	OS	OD	OD	OD	OS	OD	OS	OD	OS	–
Axial length (mm)	24.5	24.5	23.2	24.4	23.7	23.8	24.7	25.0	24.0	24.0	25.2
Fixation pressure (mmHg)	50	5	5	50	5	50	5	50	5	50	–
Area LC-Ret (mm ²)	3.0	2.7	3.1	4.0	3.6	3.3	4.3	4.3	3.6	3.6	2.9
Area LC-ON (mm ²)	3.7	3.6	3.6	4.6	4.0	3.3	4.8	4.7	4.4	4.4	3.7
Equivalent radius r_b (μm)	978	935	998	1136	1066	1033	1173	1166	1075	1073	954
Mean LC thickness (μm)	196	188	142	203	264	219	203	203	246	272	260
Mean peripapillary sclera thickness (μm)	400	380	440	430	480	470	510	490	550	540	440
Volume (μl)											
Total	13.2	15.9	15.2	18.6	22.2	21.5	24.5	26.0	22.9	19.1	30.2
ROI	10.9	11.4	11.9	13.2	12.6	15.4	14.6	15.0	14.6	14.3	8.8
Pre-laminar	2.6	2.7	2.2	2.8	2.5	3.4	2.5	3.2	3.1	2.3	2.1
Post-laminar	4.9	5.5	6.0	5.7	5.6	6.3	6.6	6.5	6.3	7.1	4.0
Sclera	1.5	1.5	1.8	2.0	1.8	3.0	2.6	2.6	2.6	2.4	1.5
Lamina	0.68	0.62	0.49	1.08	0.74	0.96	0.97	1.02	1.15	0.89	0.88
Pia	1.1	1.0	1.4	1.6	2.0	1.8	1.9	1.6	1.5	1.6	0.3

Eyes were randomly selected to be fixed at low (5 mmHg) or high (50 mmHg) IOP. All simulations were carried out for a change in IOP of 45 mmHg (5 to 50 mmHg, or vice versa). Tissue volumes are reported for tissue within the region of interest (ROI), except for total volume, which corresponds to the reconstructed volume of the entire ONH model. Also shown are the surface areas of the anterior (LC-Ret), and the posterior (LC-ON) LC surfaces to provide a sense of the shape of the LC. *OS* left eye; *OD* right eye. For details on how the LC and peripapillary sclera thickness were measured please see [Sigal \(2006\)](#)

managed in accordance with the provisions of the declaration of Helsinki for research involving human tissue. When a pair was available, one eye was randomly chosen to be fixed and reconstructed at a relatively low 5 mmHg while the contralateral eye was fixed and reconstructed at a relatively high 50 mmHg. Eyes were fixed at these pressures for another aspect of the study that is not considered herein, but that is discussed in more detail in [Sigal \(2006\)](#). A detailed description of the model construction technique has been presented in [Sigal et al. \(2005b\)](#), and refined in [Sigal et al. \(2007, 2008\)](#). In brief, photographs from stained serial sections were loaded into Amira v3.1.1 (Mercury computer systems, USA) and manually segmented to define five tissue regions: sclera, lamina cribrosa, pre and post-laminar neural tissue and pia mater. Segmented sections were then used to build a 3D reconstruction of the individual ONH.

In addition to the individual-specific models described above, we also carried out simulations with a generic (non-patient-specific) model of the optic nerve head. This model has been previously used ([Sigal et al. 2004, 2005a,b](#)), and provides a convenient reference for the individual-specific models.

2.1.2 Material properties

Material properties were assigned as for the baseline models in [Sigal et al. \(2004, 2005a\)](#). All tissues were assumed to be homogeneous, practically incompressible ($\nu = 0.49$), and linearly elastic, with Young's moduli based on direct (sclera: 3 MPa; neural tissue, both pre and post-laminar: 30 kPa) or indirect (lamina cribrosa: 300 kPa; pia mater: 3 MPa) measurements in the literature. A detailed justification of the choice of parameters is given in ([Sigal 2006](#)). We acknowledge the fundamental importance of the parameter selection and therefore have also carried out a sensitivity study on the influence of the choice of these parameters on the predictions made with individual-specific models. The results from this study are presented in the companion paper ([Sigal et al. 2008](#)).

2.1.3 Boundary conditions

Since only the ONH region was reconstructed, all models were embedded into a generic spherical shell, as described in more detail in [Sigal et al. \(2005b\)](#) and [Sigal \(2006\)](#). Our

intention was for the generic shell to provide boundary conditions that were as realistic as possible, yet equivalent for all the individual-specific models. Because previous work (Sigal et al. 2004, 2005a) has shown the importance of scleral geometric properties on ONH biomechanics, we thought it important to optimize the match in the sclera between individual-specific ONHs and a generic shell. Hence when embedding the individual-specific ONH models into the generic shells we focussed first on the best possible match of the anterior surfaces of the peripapillary sclera between the shell and the ONH; second on matching the locations of the scleral canal walls; and finally on matching the anterior and posterior surface locations of the LC itself.

We tested the embedding procedure by randomly selecting one eye, and repeating the embedding on three occasions at least 1 week apart. Each embedded ONH was then exposed to a simulated increase in IOP as for all the other models. There were slight differences in relative location and orientation of the LC between the two embeddings. Differences in location were smaller than 20 μm (smaller than 5 μm in the anterior-posterior direction), while differences in orientation were smaller than 1.5 deg. More importantly, the differences in predicted biomechanical response to an increase in IOP between both embeddings were much smaller than between predictions from models from different eyes.

In some cases the individual-specific model was not completely enclosed in space by the generic model. In such cases the displacement boundary conditions from the generic shell were spatially extrapolated. The accuracy of the extrapolations was tested by making “padded” models of the generic shell, in which a material nine orders of magnitude more compliant than the sclera was added to both the interior and exterior of the sclera, effectively increasing the scleral shell thickness without altering its compliance. These models were solved by forcing the entire sclera to deform as in a non-padded case. The differences in predicted IOP-induced displacements between extrapolations and padded models were less than 10^{-6} μm implying that the mismatch between individual-specific models and the generic shell, and the consequent boundary condition extrapolations, were unlikely to introduce errors beyond those involved in using a generic simplified shell, as described above. We conclude that the embedding procedure was sufficiently robust and repeatable.

The effects of IOP were modelled as a homogeneous force acting on the element faces exposed to the interior of the eye. Boundary conditions (displacements from the spherical shell, and forces representing IOP) were adjusted such that models reconstructed from eyes fixed at 5 mmHg were “inflated”, i.e. experienced a simulated increase in IOP to 50 mmHg by applying a positive force—outwards, while those models from eyes fixed at 50 mmHg were “deflated”, i.e. experienced a simulated decrease in IOP to 5 mmHg by applying a negative force—inwards. This simple change in boundary

conditions is applicable thanks to the assumption of linear elasticity. No other forces were applied on the models.

2.1.4 Mesh and solution

All models were meshed according to the results of the mesh refinement study described in (Sigal et al. 2005b). A typical mesh was formed by 600,000 nodes, 400,000 10-node tetrahedral elements (Solid92 in Ansys, Ansys Inc., Canonsburg, PA, USA), and 1.7 million degrees of freedom. Details of each mesh can be found in (Sigal 2006). Solutions were obtained using Ansys (Ansys Inc. Canonsburg, PA, USA) v8.1 PCG solver with default parameters, typically requiring less than 1 h of CPU time on a desktop workstation with MS Windows XP SP1 (Microsoft, Redmond, WA, USA), and an Intel 3.0GHz CPU with 4 GB of memory.

2.2 Analysis

Changes in IOP produce complex deformations of the ONH (Sigal et al. 2007, 2008). Therefore, the response of an ONH model to changes in IOP was characterized by the displacement field (the displacement in the X , Y and Z directions of each node), and the three strain modes, namely maximum extension and compression (first and third principal strains), and maximum shearing. As described in Sigal et al. (2007, 2008), we computed the maximum shear strain as the magnitude of the mean of the first and third principal strains. Using custom scripts, ONH response files were ported from Ansys to Amira for visualization and post-processing. Amira is limited to linear elements and therefore FEM results obtained on 10-node tetrahedra were mapped onto 4-node tetrahedra to allow for analysis in Amira.

The presentation of all results was standardized so that all solutions represented the effects of an increase in IOP, which simplified comparison. All displacements reported here incorporate a zeroing of the anterior–posterior displacement at the vitreo-retinal interface 5° from the axis of symmetry, and therefore are local displacements relative to this ring. This corresponds to the way that displacements are determined experimentally by confocal laser scanning imaging (see below).

The size of histologic sections from which the ONH model was created and the length of the optic nerve varied from eye to eye. To reduce variation as much as possible, and to allow fair comparison of results between models, we defined a region of interest (ROI), as described in Sigal et al. (2007, 2008). Briefly, the area of the interface between the LC and the pre-laminar neural region was computed. The radius of a disc with the same surface area was calculated (r_a). The ROI was then defined as a circular cylinder of radius $r_b = 1.5 \times r_a$, with longitudinal axis through the center of mass of the LC and parallel to the axis of symmetry of the shell used for

boundary conditions. The posterior limit to the ROI was a plane 1.5 mm posterior to the center of mass of the LC. Data on the radius of the ROI and the laminar areas from which they were computed are provided in Table 1 for each model.

The distribution of the magnitude of each strain mode, in each tissue region of each model, was computed using the method described in Sigal (2006) and Sigal et al. (2007, 2008). From these distributions we computed the 50th and 95th percentiles, representing the median and peak of the measure for the tissue region and model.

2.3 Comparison of predictions and experiments

Although it is not possible to measure the biomechanical environment within the ONH, it is possible to measure the deformations of the anterior surface of the ONH as IOP is changed. To do so, eyes were imaged with a scanning laser tomographer (Heidelberg Retinal Tomograph, HRT v2) to measure the topography of the vitreo-retinal interface prior to preparation for histology, as described in Sigal et al. (2005b). Briefly: the eyes were placed in a custom chamber filled with physiological saline, whose temperature was maintained at 37°C. By adjusting the level of a saline reservoir connected by a cannula to the interior of the eye the IOP was sequentially set to 5, 15, 22, 30, 40 and 50 mmHg above chamber pressure. At each pressure, after allowing the eye to equilibrate (viscoelastically relax), a series of 256×256 pixel images, with a 10° field of view centered on the ONH, were acquired. After imaging the IOP was set to the final level, perfusion fixed and prepared for model reconstruction. Axial length was measured using callipers, on the whole eye after cleaning and before dissection. The measurement was from the apex of the cornea to the exterior sclera at the macula.

The HRT's own glaucoma progression analysis routines were then used on the series of images at different IOPs to determine an experimental measure of IOP-induced vitreo-retinal interface displacement. ASCII dumps of the difference maps were ported from the HRT software to Amira using custom loading and scaling routines.

3 Results

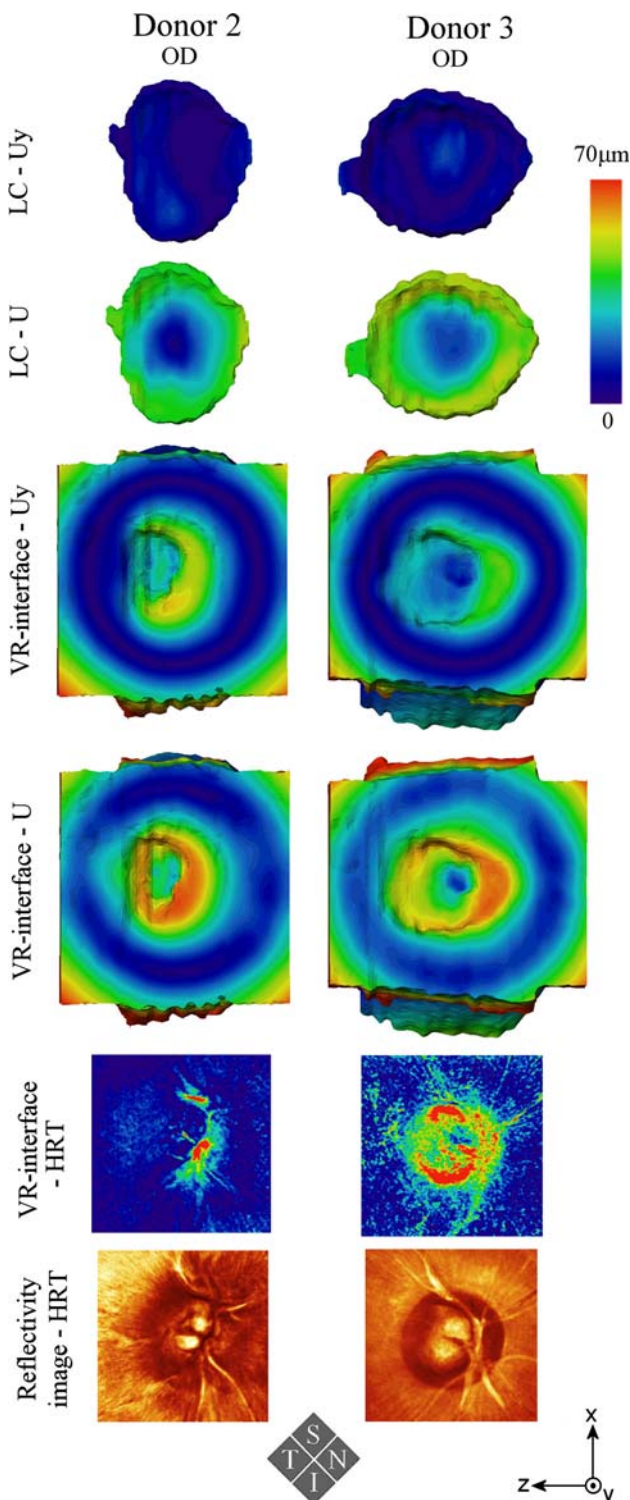
3.1 Vitreo-retinal and laminar surface deformations

Figure 2 shows the anterior surfaces of the LC from models reconstructed from the eyes of Donors 2 and 3, coloured according to the contour levels of total (U) or radial (anterior–posterior, U_y) displacements of the LC. The anterior–posterior displacements are small everywhere, whereas the total displacements are only small at the centre, implying that the tangential (U_{xz}) displacements induced by an increase in IOP from 5 to 50 mmHg are relatively large on the laminar

periphery. This is in contrast to the predicted displacements of the vitreo-retinal interface also shown in Fig. 2. Predicted displacements of the vitreo-retinal interface were generally larger in magnitude than those of the anterior surface of the LC, except at the bottom of the cup of some models (OD of Donor 3 being the clearest), where both laminar and surface displacements were small. For the vitreo-retinal interface the similarity between U_y and U implies that the tangential displacements are small. Also shown in Fig. 2 are reflectivity images and experimental measurements of displacement obtained from the eyes before preparation for model reconstruction. The reflectivity images are useful in identifying the ONH structures visible through the pupil, like the vascular tree and the optic cup. Comparison of the predicted and measured displacements of the vitreo-retinal interface shows a similar pattern. Both predicted and measured displacements are clearly not axisymmetric, being larger on the nasal side than on the temporal. Displacements on the inferior side are slightly larger than on the superior side. However, this agreement between computed and measured displacement was not observed in all eyes: in some of the eyes, very little deformation was measured with the HRT (sometimes only marginally larger than signal noise) which naturally resulted in no clear pattern of deformation. In contrast, the simulations always produced plots with clearly visible deformations.

3.2 Deformation cross sections

Figure 3 shows cross-sections through the center of the models, coloured according to the magnitude of the radial (U_y), tangential (U_{xz}) or total (U) displacements. The cross sections show details that are not clearly visible on the coronal views, such as how the small displacements of the central LC extend anteriorly to the pre-laminar neural tissue. The zeroing of the anterior–posterior displacement at 5° from the axis of symmetry appears clearly in the middle row as a dark blue region. From the plots of radial displacement in Fig. 2 (third row) it would have been possible to interpret that there are large displacements over the entire interior of the ONH. Surprisingly, the cross-sections in Fig. 3 show that anterior–posterior displacements are mostly superficial. Other regions that are posteriorly displaced are the posterior peripapillary sclera and the central optic nerve. The cross-sections also clearly show how the limited tangential displacement visible on the surface is not representative of the internal situation. These results are consistent with the decoupling of the displacements of the vitreo-retinal interface and lamina cribrosa described in Sigal et al. (2005a), and the results of Sigal et al. (2005a) are therefore likely not an artifact of the use of a generic axisymmetric geometry.



◀ **Fig. 2** Predicted and measured deformations of the lamina cribrosa and the vitreo-retinal interface due to an increase in IOP from 5 to 50 mmHg. Shown are en-face (coronal) views of model surfaces at the reconstructed IOP coloured according to the magnitude of the anterior–posterior (radial, U_y) or total (U) IOP-induced displacements. The *first two rows* show the geometry of the anterior surface of the LC. The *third and fourth rows* show the anterior surface of the model, i.e. the vitreo-retinal (VR) interface. The *fifth row* is the experimentally measured IOP-induced deformation of the vitreo-retinal interface for the same change in IOP of 45 mmHg, on the same eyes prior to preparation for reconstruction. Deformation was computed using the HRT's own glaucoma progression analysis routines. The *last row* is a reflectivity image acquired with the HRT during topography scanning. Predicted displacements are computed with respect to a reference ring on the vitreo-retinal interface 5° from the axis of symmetry, consistent with a 10° field-of-view scan. *S* Superior, *I* Inferior, *N* Nasal, *T* Temporal, *OD* Right eye, *OS* Left eye

(Geijssen 1991), IOP-induced displacements are generally smaller than $100\mu\text{m}$. As IOP increases, individual-specific models undergo complex deformations in 3D. Displacements normal to the cross section are responsible for some aspects of the more drastic changes, such as the shape of the cup in the eye of Donor 2.

Another interesting feature of the IOP-induced deformation visible in Fig. 3 is the combined effect of the lateral displacements transmitted into the ONH tissues by the peripapillary sclera, and the steep walls of the cup of the eye of Donor 3. The result is that a substantial amount of the deformation of the cup is a lateral enlargement, with very little change in depth. This kind of deformation is a challenge for the algorithms that compute deformation and remodeling of ONH tissues from sequential topography scans, like those of the HRT. We believe that better understanding of the displacements of the ONH induced by acute changes in IOP could improve analysis and evaluation of HRT scans.

3.4 Strain fields induced by an increase in IOP

Predicted strain fields on cross sections through the center of four individual-specific models as a result of an IOP increase from 5 to 50 mmHg are shown in Fig. 4. The pre-laminar neural tissue region had the highest peak levels of all three measures of strain. While the lamina cribrosa regions did not reach levels quite as high, the distribution of strain was more homogeneous, making the lamina the region with the highest median levels of strain. There were also some regions of high strain in the post-laminar neural tissue region (the optic nerve), generally in the periphery near the meeting point of the lamina cribrosa, the pia mater, the sclera and the optic nerve. However, the large volume of post-laminar neural tissue leads to a low median level of strain compared with the laminar or pre-laminar regions. The scleral tissue had the most homogeneous distribution of strain, whereas the pia mater had some high strains near the boundary with

3.3 Vector plots of displacement and deformed geometries

The direction of displacement and the change in geometry produced by the increase in IOP are better understood through the vector plots of the fourth row of Fig. 3. Even for a physiologically large increase in IOP from 5 to 50 mmHg

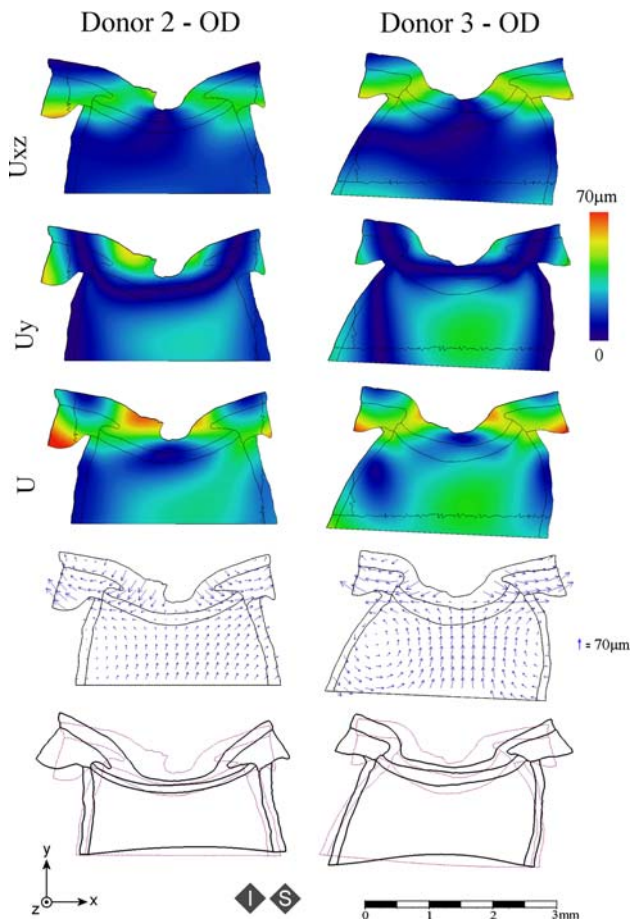


Fig. 3 Sagittal cross-sections through the center of the models reconstructed from the eyes of Donors 2 and 3. The *top three rows* are coloured according to the magnitude of predicted deformation for an increase in IOP from 5 to 50 mmHg. The *three first rows* differ in the component of the deformation coded in colour: the total magnitude of the displacement (U), the radial (U_y , anterior–posterior) component, or the tangential (U_{xz} , the vector magnitude of the superior-inferior U_x , and nasal-temporal U_z). Note the large tangential displacements internal to the ONH, which are often not visible from the surface. The *fourth row* shows the displacement vectors at the point of origin of the vector. The vectors were computed in 3D, with their 2D projections shown. Vector lengths are proportional to the magnitude of the total displacement, with the scale exaggerated for clarity. In the *first four rows* the *black lines* are the outlines of the tissues (*smooth lines*) or the region of interest (*jagged lines*). The bottom row shows outlines of the models at 5 mmHg (*thin purple line*), and at 50 mmHg (*thick black line*). Deformations are exaggerated fivefold for clarity. Visible are effects such as the rotation of the sclera, the flattening of the cup, the thinning of the LC and pre-laminar neural tissues and the anterior movement of the central regions of the optic nerve relative to the LC. Also clearly visible are the zeroing of the anterior-posterior displacement 5° from the axis of symmetry. S Superior, I Inferior

the sclera, but elsewhere the strain was low. Consistent with previous results (Sigal et al. 2007, 2008), the largest predicted strain levels occur in compression, followed by shear and finally in extension. All three modes of strain shown reach relatively high levels within the neural and laminar regions. From the figures it is clear that there are differ-

ences between the distributions of the various modes of strain within a model, on the same mode of strain between models, and even in models from contralateral eyes. There are also some similarities in the strain distributions between different models, such as a high-compression region directly anterior to the center of the LC, and another smaller high-compression region posterior to the peripheral LC.

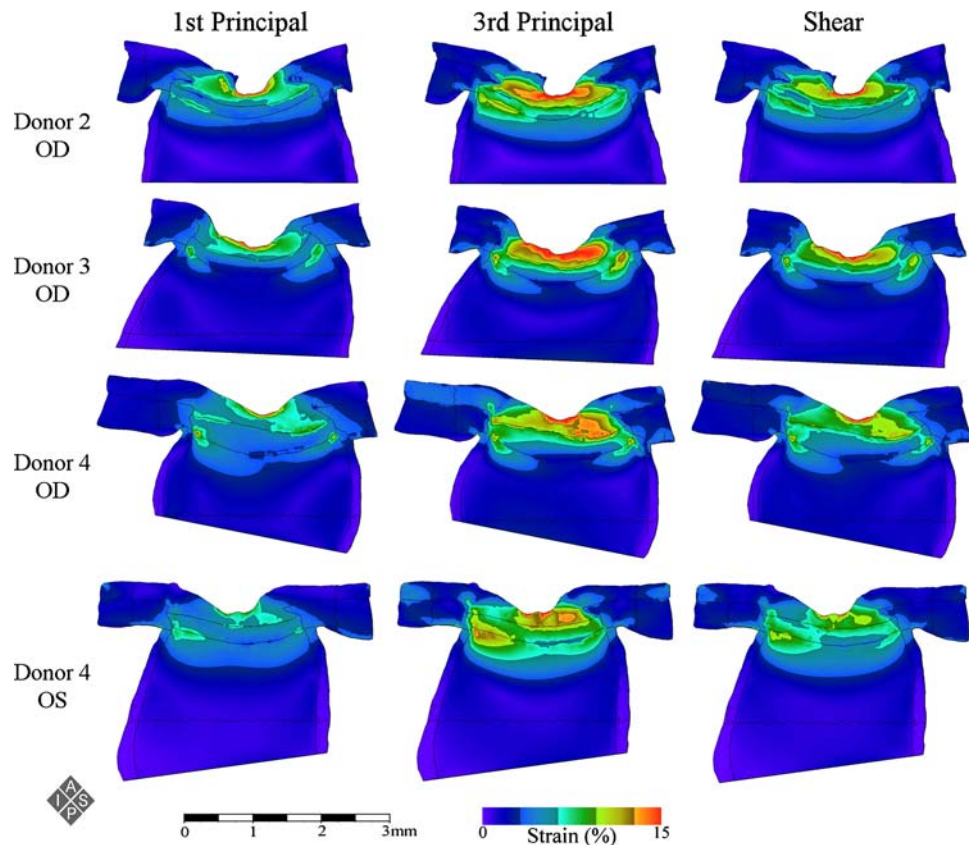
Previous parametric studies (Sigal et al. 2005a) identified globe size, lamina cribrosa thickness and peripapillary scleral thickness as having important influences on ONH biomechanics. As can be seen from Table 1, previous generic models used values of these parameters that fell within the measured range from individual-specific models, except that the peripapillary sclera tended to be slightly thinner in the generic eye than in the individual-specific models. Nonetheless, this did not lead to a generic model with higher ONH strains than the individual-specific models, likely because the thinner peripapillary sclera in the generic eye occurred only in the region immediately adjacent to the canal. More generally, we were unable to observe any clear systematic relationship between laminar or scleral thicknesses and level of stress or strain in the ONH for the individual-specific models. Because morphometry in 3D is very complex, and because there are potentially many geometric factors that could influence ONH biomechanics in individual-specific models, it was outside the scope of this paper to systematically look for quantitative correlations between geometric factors and ONH biomechanics in our individual-specific models.

3.5 Median and peak levels of strain

Figure 5 compares the distributions of three modes of strain, across the 11 models (10 individual-specific and 1 3D generic model). There was no clear pairing of the distributions from models of paired eyes. The median and peak values of each mode of strain within each tissue region of each model are presented in Fig. 6.

Compared to other ONH tissues, the sclera is stiff, resulting in low and homogeneous strains, as can be seen by the relatively constant and low level of the median and peak values for all eyes and strain modes (bottom row of Fig. 6). For the more compliant tissues, the strain levels are higher and less homogeneous. The post laminar neural tissue median levels are not higher than in the sclera, but the peak values are much higher and much more variable, revealing concentrations of high strain. The large differences between median and peak strain are even larger in the pre-laminar neural region, where not only are the median levels high, but the peak levels are the highest within the ONH (for all eyes, except the generic model, as will be discussed below). Although the pre-laminar neural tissue regions reach higher strain levels, the median strain is substantially higher within the LC than in the pre-laminar neural tissue region.

Fig. 4 Contour plots of three modes of strain predicted for several individual-specific models for an increase in IOP from 5 to 50 mmHg. For each eye all sections are the same sagittal section through the center of the model, differing only in the contoured quantity. *S* Superior; *I* Inferior; *A* Anterior; *P* Posterior. Extension and compression are the first and third principal strains, respectively



When comparing the distributions of strain in Fig. 5, and the median and peak levels of strain in Fig. 6 with the contour plots of Fig. 4, it is important to remember that the contour plots are shown only on one sagittal cross-section through the center of the models, and distributions, median and peak values are computed over the whole ROI, so that regions that appear identical in area in a contour plot could represent very different volumes. An effect similar to that discussed in Sigal et al. (2004, 2005a) for axisymmetric generic models is taking place: regions near the axis of symmetry represent relatively small volumes, whereas those further from the axis represent much larger volumes. Concentrations of strain on the bottom of the cup occur on a small volume, and therefore may have more effect on the peak than on the median values. Conversely, apparently modest increases in strain in peripheral regions could have a substantial effect on the median without much effect on the peak values.

4 Discussion and conclusions

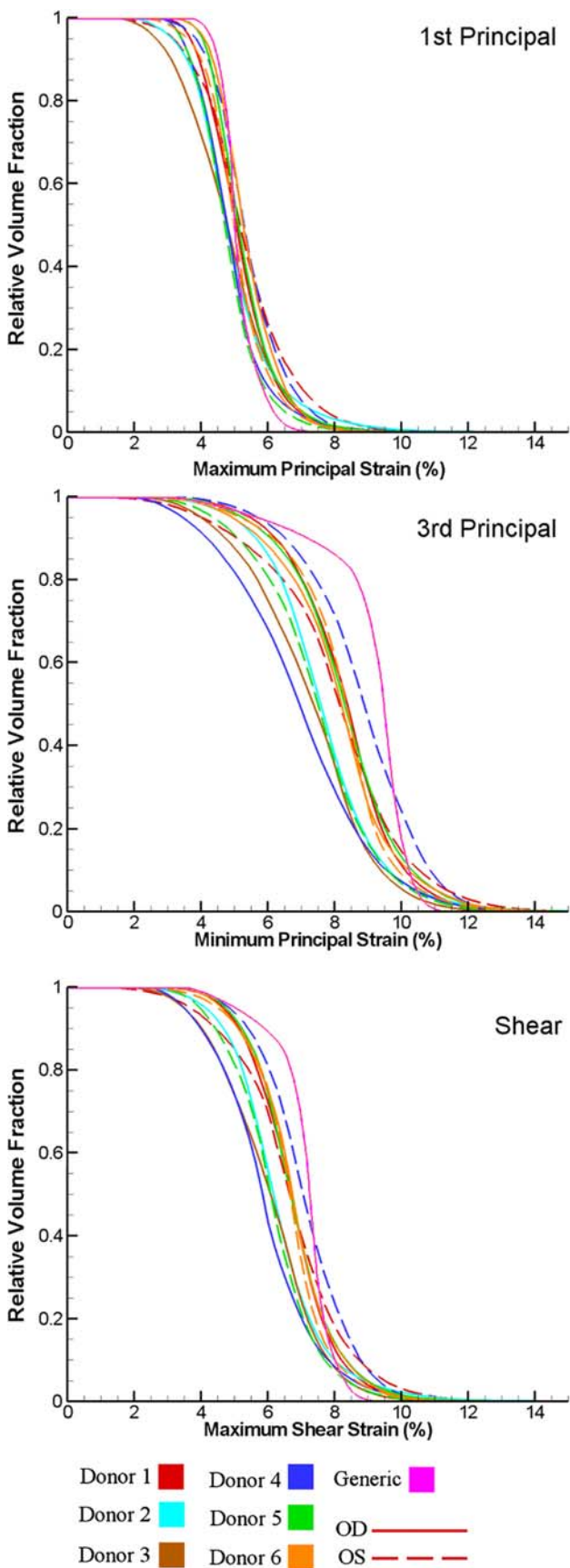
4.1 Summary and main results

Although not numerous compared with the over 500 models considered in Sigal et al. (2005a), the 10 individual-specific models considered in this work are a very important set;

namely a group of real ONHs, which represent an advance over generic models. Use of individual-specific geometries corresponds to varying collectively all the geometric parameters that change from one individual to another, whether the relationships between geometric input factors are known or not, and therefore allows us to assess the importance of geometric factors on ONH biomechanics in a physiologically meaningful way.

4.1.1 The models differ little in median predicted strain and only slightly in peak predicted strain

Our main conclusion is that the geometry of an ONH has only a modest effect on the median and peak levels of the three measures of strain in ONH tissues. As will be seen from the companion paper, material properties have a much larger effect on ONH strains (Sigal et al. 2008). Overall the levels of strain predicted for the pre and post-laminar and laminar tissue were potentially biologically significant, but as discussed in Sigal et al. (2007, 2008), to the best of our knowledge, the levels and modes of strain that have physiologic relevance in each tissue are still unknown, as is whether the physiologically relevant measure is the median or the peak. Downs et al. (2003) proposed that levels of strain above 3.5% could be pathophysiological. Slightly higher strain levels (5–6%) were sufficient to induce a wide range



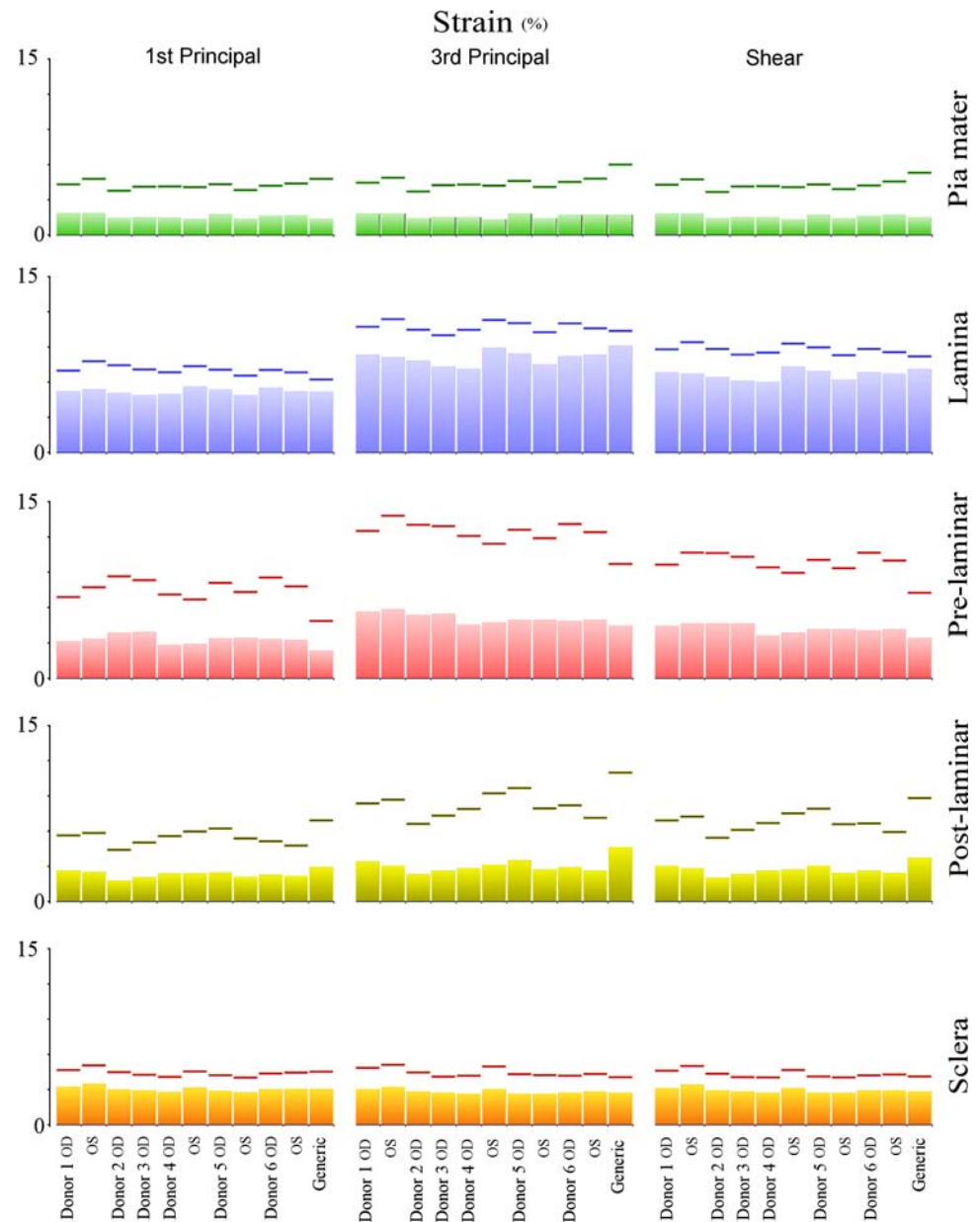
◀ **Fig. 5** Comparison of the distribution of first principal strain (*top*), third principal strain (*middle*), and maximum shearing strain (*bottom*) within the lamina cribrosa of all individual-specific models plus the Generic Model. Each curve represents the fraction of lamina cribrosa tissue volume (y axis) that has a level of strain below a certain level (x axis). From curves like these we computed the median (50th percentile) and peak (95th percentile) levels. Models with homogeneous distributions of a measure would have a steep curve, with similar median and peak levels. As the distribution becomes less homogeneous the curve becomes more horizontal, and the median and peak levels separate. While the distributions of first principal strain (extension) for all models are quite similar and are difficult to tell apart in the plot, those of third principal strain (compression) have some clear differences. The curves for the Generic Model reveal higher levels of third principal strain than in the individual-specific models. Lines from the eyes of the same donor do not appear to pair; see for example the blue lines from Donor 5, which bracket all others in the middle plot

of biological effects in neuronal cells in in vitro models (Edwards et al. 2001, Triyoso and Good 1999). The same threshold for axonal injury was observed by Margulies and Thibault (1992). Using adult guinea pig optic nerves Bain and Meaney (2000) estimated a Lagrangian strain threshold of 21% for morphological axonal injury, and 18% for deterioration of nerve function. Several mechanisms by which strain could be transduced into physiologic effects have been proposed, including disruptions in cell adhesion, transmembrane transport and RNA processing (Ellis et al. 1995, Hernandez 2000), or in laminar astrocytes due to microtubule loss from transient stretch injury (Jafari et al. 1997). The peak levels of strain predicted by our models exceed most of the threshold values quoted above, and this is without considering the micro-structure of the LC that could “amplify” strain as it is transferred from the extracellular matrix (ECM) to the mechanically sensitive structures (RGC axons or LC astrocytes, for example)!

It is still unclear which variations in geometry between models lead to the differences in predicted mechanical response to IOP. All models have been solved using the same material properties, and assigned boundary conditions from the same generic axisymmetric model. Nevertheless, the predictions for the models are not identical and the origins of these differences must be the geometry of the ONH. This shows that ONH geometry does have an effect on ONH biomechanics, albeit a modest one. However, the causal link between a specific geometric feature and the resulting mechanical response is still unclear.

We recognize that as defined in this work, the maximum shear strain has a magnitude intermediate between that of the first and third principal strains, and is therefore not an independent strain measure. Nonetheless, we have included plots of this quantity to avoid readers having to mentally compute shearing strain distributions from plots of first and third principal strains, and because researchers in the ocular biomechanics area have an intuitive understanding of

Fig. 6 Comparison of median (50th percentile, *bars*) and peak (95th percentile, *lines*) over the five tissue regions for all ten individual-specific models and the generic model 3. Three measures of strain are displayed: first principal strain (extension), third principal strain (compression) and maximum shearing strain (shear). For the neural and lamellar tissues the strain reaches potentially biologically significant levels (Kirwan et al. 2005). Generally, differences between models are relatively small for the peak values, and even smaller for the median values. The difference between the median and peak levels of a measure for a tissue region provides a rough measure of the level of homogeneity of the measure within the tissue



shearing strain that is reflected in many discussions of the possible pathologic role of this quantity in mechanically insulating the retinal ganglion cell axons in the lamina cribrosa (Burgoyne et al. 2005, Edwards et al. 2001, Hernandez 2000, Levy and Crapps 1984, Yan et al. 1994).

4.1.2 Predicted deformations have both tangential and radial displacements, with substantial differences between the retinal and lamellar surfaces

Due to the difficulties in accessing the ONH directly, studies of ONH biomechanics often use the vitreo-retinal interface as a surrogate for the ONH interior. To assess this assumption we compared the predicted IOP-induced displacements at the

vitreo-retinal interface with those in the internal ONH, and more specifically, with the anterior surface of the lamina cribrosa. Our data show substantial differences in IOP-induced displacements at these two locations. It is sometimes thought that the anterior surface of the lamina cribrosa can be seen in optic disc photographs, which is probably what has encouraged some researchers to suggest that the displacements of the vitreo-retinal interface they measure with an HRT correspond to those of the anterior surface of the lamina (Maeda et al. 1999, Miller and Quigley 1988). Although intuitively reasonable, the results from the present study clearly indicate that such arguments can lead to erroneous conclusions. Only at the bottom of the cup of highly cupped eyes did our models predict similar displacements for the vitreo-retinal interface

and the anterior lamina cribrosa. For example, while displacements of the vitreo-retinal interface are mostly anterior–posterior, those of the anterior lamina surface are tangential (nasal–temporal and superior–inferior). Tangential LC displacements are also the result of deformation transmitted to the LC by the peripapillary sclera, and exhibit the importance of boundary conditions in ONH biomechanics. Most models predict a very small displacement of the central lamina cribrosa, with the periphery displacing mostly tangentially (in the superior–inferior and nasal–temporal direction). However, it is important to consider that our models simulate an acute increase in IOP, and do not consider the remodeling process in glaucoma, where the displacements of the vitreo-retinal interface and the anterior laminar surface could match better.

The above is not meant to imply that current imaging technology is not clinically relevant (it is), but rather to evaluate whether current imaging methods capture the fundamental aspects of ONH biomechanics. Our results suggest that they do not. Our intention here is twofold: to encourage further development of imaging technologies and techniques, and to promote the analysis and evaluation of the ONH from a biomechanical perspective that considers the limitations of current imaging. Our conclusions based on individual-specific models agree with previous findings from axisymmetric models.

In general, differences between individual-specific models and the generic axisymmetric model were not much larger than differences between any two individual-specific models, consistent with observations described in Sigal et al. (2005b, 2007, 2008). This suggests that the conclusions derived using generic axisymmetric models presented in Sigal et al. (2004, 2005a) likely extend to individual-specific models, as a good first approximation. An obvious exception to this comment is that the response of individual-specific models was asymmetric.

4.2 Limitations

The limitations of the process of reconstruction and finite element modeling of individual-specific optic nerve heads have been discussed in length in Sigal et al. (2005b, 2007, 2008). These include the material properties, resolution and general quality of the reconstruction, model meshing, solution methods, boundary conditions, analysis and others. It is not our intention to discuss them at length again. Instead we focus below on limitations and considerations particular to this work.

4.2.1 All individual-specific models are embedded in the same generic shell for boundary conditions

Previous studies on axisymmetric models (Sigal et al. 2004, 2005a) have suggested that ONH biomechanics are strongly

influenced by the properties of the peripapillary sclera (including its thickness, its stiffness, the radius of the ocular shell and to a lesser degree the scleral shape directly adjacent to the canal). Thus, fitting all individual-specific models to the same generic model shell might reduce the differences that eye anatomy could have on the mechanical response of an ONH. Still, the objective of this work was to study the effects of differences in ONH anatomy, not of whole eye anatomy in ONH biomechanics. Using the same boundary conditions for all models we were able to “level the field” and do a fair comparison between the ONH models. The relatively large role of scleral geometry identified in previous work suggests that extending the individual-specific models to include scleral shell thickness could increase inter-individual variations in predicted ONH biomechanics and help uncover the origin of differences in susceptibility to IOP.

The relatively good agreement between generic and individual-specific lamina cribrosa geometry, location and orientation presented in Sigal (2006) suggests that the ONH geometry of the generic model used for boundary conditions is likely adequate in the sense defined in Sigal et al. (2005b), and that the relative orientation of the individual-specific models and the generic shell was acceptable.

The loading applied to the ONH was somewhat simplified in this study. We have previously considered more complex boundary conditions, for example including the forces exerted by the cerebro-spinal fluid pressure (CSFp), extending the post-laminar neural tissue, or inserting a simplified blood vessel (Sigal et al. 2004, Sigal 2006). None of these had substantial effects on predictions obtained using generic axisymmetric models. The small effects of CSFp were likely due to a combination of effects: First, because IOP acts on a much larger surface than CSFp, and therefore the effects of IOP on the ONH have the two contributions discussed in the manuscript: the direct effect of IOP on the ONH, and the indirect effects of IOP transmitted to the ONH through the scleral shell. Second, the LC is concave as seen from the interior of the eye, which provides a more stable shape to forces from the exterior of the eye than from the interior. Finally, although both IOP and CSFp vary, CSFp is usually much lower than IOP.

The optic nerve adopts a sinuous form, where the nerve is neither in significant tension or compression (Bain and Meaney 2000). The forces transmitted to the eyeball through the optic nerve have been studied and found to be much smaller than those of other forces acting on the eye (Cirovic et al. 2005, 2006, Schutte et al. 2006, Schoemaker et al. 2006), and it is therefore acceptable to ignore the effects of nerve tension.

Recall also that the measurements obtained using the HRT on the donor eyes did not include CSFp, since the optic nerve was cut a few mm behind the LC, and the blood vessels were not pressurized. Therefore to allow a fair comparison

with the experiments we decided not to include any of these effects in the simulations shown in this work. Nevertheless we acknowledge that in studies in dogs where CSFp has been artificially raised to very high levels while using an HRT to track the topography of the ONH significant changes have been measured, suggestive of anterior displacements of the LC as CSFp increases (Morgan et al. 2002).

All the eyes were assumed to be healthy; however, considering the donors ages we cannot exclude the possibility that some eyes had pre-existing optic neuropathy that was not notified to the eye bank.

4.2.2 Arbitrariness of the ROI

To allow comparison between individual-specific models, and to reduce the effects of the arbitrariness in the location of the boundaries of the individual-specific ONHs, a region of interest (ROI) was defined for each model. The definition of the ROI based on the area of the anterior lamina cribrosa was intended to focus on the anatomy of the lamina cribrosa, and although reasonable, it was still arbitrary. It is possible that in the future this definition of the ROI will have to be revised. The ROI contains the full LC, but only partial volumes of all other tissues, and therefore a larger ROI decreases the median and peak levels of strain within all regions except the LC.

4.2.3 Differences between predicted and measured vitreo-retinal interface IOP-induced displacement

Predicted vitreo-retinal interface displacements agreed well with measured displacements for some eyes, and less well for others. More specifically, when a clear pattern of deformation was measured with the HRT, which was the case in about one-third of the eyes, the numerical simulations reproduced the deformation pattern reasonably well, albeit sometimes at a slightly different magnitude (Fig. 2). However, in some eyes, experiments showed no discernible effect of increased IOP, while the finite element models still predicted some displacement.¹ These differences could be, in part, because contour plots from simulations are not obscured by the noise present in HRT measurements, which could make patterns more easily discernible in the models than in the experiments. They could also be due to the assumed material properties of the tissues, as discussed in Sigal et al. (2005b, 2007, 2008). But there are also potential problems with the way in which the HRTs glaucoma progression analysis routines identify deformation, as discussed more fully in Sigal (2006). We believe

¹ “No discernible effect of IOP” meant that the measured displacement was smaller than the noise in the HRT-measured topography, where noise magnitude was estimated from the roughness of smooth regions surrounding the ONH.

that cases where discrepancy exists between experiments and computations may be due to inter-individual differences in material properties, as discussed in more detail in the companion paper (Sigal et al. 2008).

4.2.4 Material properties

The adequacy of the tissue material properties used in this study is a very important issue that has been discussed in detail elsewhere (Sigal et al. 2004, 2005a, Sigal 2006). All the individual-specific models in this study were assigned and solved with the same material properties, namely, the baseline values used in the parametric and sensitivity analysis of Sigal et al. (2005a). A sensitivity analysis of the effects of variations in material properties on individual-specific models is presented in the companion paper (Sigal et al. 2008). Important in this context are the Poisson ratios of the constituent tissues, since these may affect compressive strains. Little data exist for these Poisson ratios, except for several measurements in the literature that show that the sclera is nearly incompressible (Battaglioli and Kamm 1984, Stitzel et al. 2002, Uchio et al. 1999). Soft tissues composed mostly of water are generally regarded as incompressible; however, over long time scales (such as those relevant in glaucoma), water content can change due to effects such as interstitial fluid movement, altered blood perfusion, or axoplasmic flow. In the companion paper we investigate the sensitivity of our results to changes in the Poisson ratio of the pre-laminar tissue. Recent work on poroelastic properties of the scleral tissue may eventually help characterize the time scales associated with fluid displacement and volume changes within the sclera and ONH tissues (Simon et al. 2006, Vande Geest et al. 2007), and this issue should be re-examined when better data becomes available.

When discussing material properties, it is particularly interesting to consider the refractive status of the eye. There is evidence from animal models that there is an association between refractive status and scleral properties, including some aspects of scleral mechanics (Norton and Rada 1995, Rada et al. 2006, Siegwart and Norton 1999). This is of interest since scleral mechanical properties have been shown to be important in ONH biomechanics (Sigal et al. 2005a). Unfortunately we did not have information about the refractive status of the donors eyes in this study, as this is almost never available to the eye bank. We have instead included information about the axial length as an indirect proxy for refractive status (Table 1). We did not observe any relationship between axial length and ONH biomechanical response, but this issue should be examined in further studies.

Although the results presented here were computed for an acute increase in IOP from 5 to 50 mmHg, responses to any change in IOP can be readily estimated by linear interpolation. This could be useful, for example, when studying

the most common type of glaucoma (chronic glaucoma), in which moderate elevations in IOP are sustained for years.

4.3 Relevance

These results show that the levels of strain predicted for ONHs with different anatomies are relatively consistent. However, the results should not be understood as suggesting that differences in anatomy could not play any role in explaining the wide range of susceptibilities to IOP that is seen clinically. For example, small differences in strain, if sustained over many years, could be sufficient to produce a range of effects. Nonetheless, these data suggest that factors other than inter-individual differences in ONH anatomy should be investigated to explain differing susceptibilities to elevated IOP.

Acknowledgments This work was supported by the Consejo Nacional de Ciencia y Tecnologia de Mexico (IAS), the Canadian Institutes for Health Research (CRE, JGF), the Canada Research Chairs Program (CRE) and Glaucoma Research Society of Canada. We thank the Eye Bank of Canada for providing donor tissue.

References

- Bain AC, Meaney DF (2000) Tissue-level thresholds for axonal damage in an experimental model of central nervous system white matter injury. *J Biomech Eng* 122(6):615–622
- Battaglioli JL, Kamm RD (1984) Measurements of the compressive properties of scleral tissue. *Invest Ophthalmol Vis Sci* 25(1):59–65
- Bellezza AJ (2002) Biomechanical properties of the normal and early glaucomatous optic nerve head: an experimental and computational study using the monkey model. Department of Biomedical Engineering, Tulane University, New Orleans
- Burgoyne CF, Downs JC, Bellezza AJ, Hart RT (2004) Three-dimensional reconstruction of normal and early glaucoma monkey optic nerve head connective tissues. *Invest Ophthalmol Vis Sci* 45(12):4388–4399
- Burgoyne CF, Downs JC, Bellezza AJ, Suh JK, Hart RT (2005) The optic nerve head as a biomechanical structure: a new paradigm for understanding the role of IOP-related stress and strain in the pathophysiology of glaucomatous optic nerve head damage. *Prog Retin Eye Res* 24(1):39–73
- Cirovic S, Bhola RM, Hose DR, Howard IC, Lawford PV, Parsons MA (2005) A computational study of the passive mechanisms of eye restraint during head impact trauma. *Comput Methods Biomech Biomed Engin* 8(1):1–6
- Cirovic S, Bhola RM, Hose DR et al (2006) Computer modeling study of the mechanism of optic nerve injury in blunt trauma. *Br J Ophthalmol* 90(6):778–83
- Downs JC (2002) Experimental and computational modeling of the posterior scleral shell of the normal and glaucomatous monkey eye. Department of biomedical engineering. Tulane University, New Orleans, p 221
- Downs JC, Suh JK, Thomas KA, Bellezza AJ, Burgoyne CF, Hart RT (2003) Viscoelastic characterization of peripapillary sclera: material properties by quadrant in rabbit and monkey eyes. *J Biomech Eng* 125(1):124–131
- Edwards ME, Good TA (2001) Use of a mathematical model to estimate stress and strain during elevated pressure induced lamina cribrosa deformation. *Curr Eye Res* 23(3):215–225
- Edwards ME, Wang SS, Good TA (2001) Role of viscoelastic properties of differentiated SH-SY5Y human neuroblastoma cells in cyclic shear stress injury. *Biotechnol Prog* 17(4):760–767
- Ellis EF, McKinney JS, Willoughby KA, Liang S, Povlishock JT (1995) A new model for rapid stretch-induced injury of cells in culture: characterization of the model using astrocytes. *J Neurotrauma* 12(3):325–339
- Ethier CR, Johnson M, Ruberti J (2004) Ocular biomechanics and bio-transport. *Annu Rev Biomed Eng* 6:249–73
- Geijssen HC (1991) Studies on normal pressure glaucoma. Kugler Publications, Amsterdam
- Heijl A, Leske MC, Bengtsson B, Hyman L, Bengtsson B, Hussein M (2002) Reduction of intraocular pressure and glaucoma progression: results from the Early Manifest Glaucoma Trial. *Arch Ophthalmol* 120(10):1268–79
- Hernandez MR (2000) The optic nerve head in glaucoma: role of astrocytes in tissue remodeling. *Prog Retin Eye Res* 19(3):297–321
- Jafari SS, Maxwell WL, Neilson M, Graham DI (1997) Axonal cytoskeletal changes after non-disruptive axonal injury. *J Neurocytol* 26(4):207–221
- Kirwan RP, Fenerty CH, Crean J, Wordinger RJ, Clark AF, O'Brien CJ (2005) Influence of cyclical mechanical strain on extracellular matrix gene expression in human lamina cribrosa cells in vitro. *Mol Vis* 11:798–810
- Levy NS, Crapps EE, Bonney RC (1981) Displacement of the optic nerve head. Response to acute intraocular pressure elevation in primate eyes. *Arch Ophthalmol* 99(12):2166–2174
- Levy NS, Crapps EE (1984) Displacement of optic nerve head in response to short-term intraocular pressure elevation in human eyes. *Arch Ophthalmol* 102(5):782–786
- Maeda H, Nakamura M, Yamamoto M (1999) Morphometric features of laminar pores in lamina cribrosa observed by scanning laser ophthalmoscopy. *Jpn J Ophthalmol* 43(5):415–421
- Margulies SS, Thibault LE (1992) A proposed tolerance criterion for diffuse axonal injury in man. *J Biomech* 25(8):917–923
- Miller KM, Quigley HA (1988) The clinical appearance of the lamina cribrosa as a function of the extent of glaucomatous optic nerve damage. *Ophthalmology* 95(1):135–138
- Morgan WH, Yu DY, Cooper RL, Alder VA, Cringle SJ, Constable IJ (1995) The influence of cerebrospinal fluid pressure on the lamina cribrosa tissue pressure gradient. *Invest Ophthalmol Vis Sci* 36(6):1163–1172
- Morgan WH, Chauhan BC, Yu DY, Cringle SJ, Alder VA, House PH (2002) Optic disc movement with variations in intraocular and cerebrospinal fluid pressure. *Invest Ophthalmol Vis Sci* 43(10):3236–3242
- Norton TT, Rada JA (1995) Reduced extracellular matrix in mammalian sclera with induced myopia. *Vision Res* 35(9):1271–1281
- Quigley HA, Broman AT (2006) The number of people with glaucoma worldwide in 2010 and 2020. *Br J Ophthalmol* 90(3):262–267
- Rada JA, Shelton S, Norton TT (2006) The sclera and myopia. *Exp Eye Res* 82(2):185–200
- Schoemaker I, Hoefnagel PP, Mastenbroek TJ et al (2006) Elasticity, viscosity, and deformation of orbital fat. *Invest Ophthalmol Vis Sci* 47(11):4819–4826
- Schutte S, Bedem SPvan den, Keulen Fvan, Helm FCvan der, Simonsz HJ (2006) A finite-element analysis model of orbital biomechanics. *Vision Res* 46(11):1724–1731
- Sieglwart JT Jr, Norton TT (1999) Regulation of the mechanical properties of tree shrew sclera by the visual environment. *Vision Res* 39(2):387–407

- Sigal IA, Flanagan JG, Tertinegg I, Ethier CR (2004) Finite element modeling of optic nerve head biomechanics. *Invest Ophthalmol Vis Sci* 45(12):4378–4387
- Sigal IA, Flanagan JG, Ethier CR (2005a) Factors influencing optic nerve head biomechanics. *Invest Ophthalmol Vis Sci* 46(11):4189–4199
- Sigal IA, Flanagan JG, Tertinegg I, Ethier CR (2005b) Reconstruction of human optic nerve heads for finite element modeling. *Technol Health Care* 13(4):313–329
- Sigal IA (2006) Human optic nerve head biomechanics: an analysis of generic and individual-specific models using the finite element method. Department of Mechanical and Industrial Engineering, University of Toronto, Toronto
- Sigal IA, Flanagan JG, Tertinegg I, Ethier CR (2007) Predicted extension, compression and shearing of optic nerve head tissues. *Exp Eye Res* 85(3):312–322
- Sigal IA, Flanagan JG, Tertinegg I, Ethier CR (2008) Modeling individual-specific human optic nerve head biomechanics. Part II: influence of material properties. *Biomechan Model Mechanobiol*. doi:10.1007/s10237-008-0119-0
- Simon BR, Rigby PH, Park RI, Basavanthappa S, Vande Geest JP (2006) Porohyperelastic experimental models for ocular tissues in unconfined and confined compression. E-Abstract 1231. ARVO, Ft. Lauderdale
- Stitzel JD, Duma SM, Cormier JM, Herring IP (2002) A nonlinear finite element model of the eye with experimental validation for the prediction of globe rupture. *Stapp Car Crash J* 46:81–102
- Triyoso DH, Good TA (1999) Pulsatile shear stress leads to DNA fragmentation in human SH-SY5Y neuroblastoma cell line. *J Physiol* 515(Pt 2):355–365
- Uchio E, Ohno S, Kudoh J, Aoki K, Kisielewicz LT (1999) Simulation model of an eyeball based on finite element analysis on a supercomputer. *Br J Ophthalmol* 83(10):1106–1111
- Vande Geest JP, Simon BR, Park RI, Rigby PH (2007) Comparison of poroelastic and elastic finite element models of normal and glaucomatous conditions in the eye. E-Abstract 3303. ARVO, Ft. Lauderdale
- Whitmore AV, Libby RT, John SW (2005) Glaucoma: thinking in new ways—a role for autonomous axonal self-destruction and other compartmentalised processes. *Prog Retin Eye Res* 24(6):639–62
- Yan DB, Coloma FM, Metheerairut A, Trope GE, Heathcote JG, Ethier CR (1994) Deformation of the lamina cribrosa by elevated intraocular pressure. *Br J Ophthalmol* 78(8):643–648